Role of hydrodynamic viscosity on phonon transport in suspended graphene

Xun Li[1] and Sangyeop Lee[1,2,*]

[1]*Department of Mechanical Engineering and Materials Science, University of Pittsburgh, Pittsburgh, Pennsylvania 15261, USA*

[2]*Department of Physics and Astronomy, University of Pittsburgh, Pittsburgh, Pennsylvania 15261, USA*

(Received 29 December 2017; revised manuscript received 14 March 2018; published 30 March 2018)

When phonon transport is in the hydrodynamic regime, the thermal conductivity exhibits peculiar dependences on temperatures (T) and sample widths (W). These features were used in the past to experimentally confirm the hydrodynamic phonon transport in three-dimensional bulk materials. Suspended graphene was recently predicted to exhibit strong hydrodynamic features in thermal transport at much higher temperature than the three-dimensional bulk materials, but its experimental confirmation requires quantitative guidance by theory and simulation. Here we quantitatively predict those peculiar dependences using the Monte Carlo solution of the Peierls-Boltzmann equation with an *ab initio* full three-phonon scattering matrix. Thermal conductivity is found to increase as T^{α} where α ranges from 1.89 to 2.49 depending on a sample width at low temperatures, much larger than 1.68 of the ballistic case. The thermal conductivity has a width dependence of $W^{1.17}$ at 100 K, clearly distinguished from the sublinear dependence of the ballistic-diffusive regime. These peculiar features are explained with a phonon viscous damping effect of the hydrodynamic regime. We derive an expression for the phonon hydrodynamic viscosity from the Peierls-Boltzmann equation, and discuss the fact that the phonon viscous damping explains well those peculiar dependences of thermal conductivity at 100 K. The phonon viscous damping still causes significant thermal resistance when a temperature is 300 K and a sample width is around 1 μm, even though the hydrodynamic regime is not dominant over other regimes at this condition.

DOI: 10.1103/PhysRevB.97.094309

I. INTRODUCTION

Graphene has extremely high thermal conductivity and thus has a great potential for thermal management applications. Past experimental studies [1,2] show that the thermal conductivity is around 4000 W/m K (up to 5300 W/m K) at room temperature for suspended graphene, and can still be as high as 600 W/m K when graphene is supported by a substrate. This high thermal conductivity is explained by graphene's large debye temperature resulting from the small atomic mass of carbon and strong carbon-carbon bonding [3]. The high debye temperature leads to large group velocity of acoustic phonon modes. In addition, phonons are predominantly populated near the center of the first Brillouin zone, leading to weak Umklapp three-phonon scattering (hereafter U-scattering). As a result, the mean free path (MFP) for U-scattering is long and even comparable to a sample size. Thus, this extremely high thermal conductivity has been discussed in between a diffusive regime and a ballistic regime [3,4].

The hydrodynamic regime is considered another important regime of phonon transport in suspended graphene [5,6]. The hydrodynamic regime requires that normal scattering (hereafter N-scattering), which conserves total momentum, is stronger than U-scattering. The suspended graphene can satisfy this condition owing to its extremely large anharmonicity of flexural acoustic phonon modes at small wave vectors [7] and high debye temperature. Both features together can cause strong N-scattering and its rate is larger than that of U-scattering by at least one order of magnitude [8]. This strong N-scattering leads to a new transport regime, called hydrodynamic phonon transport, much different from the ballistic and diffusive regimes [5,6]. Similar phenomena were predicted for other graphitic materials, such as single-wall carbon nanotubes [9] and graphite [10].

The N-scattering is similar to the intermolecular scattering in fluid flow in the sense that both scattering processes conserve total momentum of particles. As a result, the macroscopic transport phenomena are also similar in hydrodynamic phonon flow and fluid flow. The equilibrium distribution under strong N-scattering is the displaced Bose-Einstein distribution [11], similar to the Maxwell distribution displaced by a drift velocity in fluid flow. Another representative macroscopic phenomenon is Poiseuille flow. The Poiseuille flow is a fully developed steady-state flow of molecules or phonons. The driving force of molecule flow is a pressure gradient while phonon flow is driven by temperature gradient. A noteworthy difference between the phonon Poiseuille flow and the common diffusive phonon flow governed by Fourier's law is the mechanism of thermal resistance. While U-scattering directly causes thermal resistance in the diffusive flow, the thermal resistance in the phonon Poiseuille flow is due to viscous effects. The viscous effects occur when the drift velocity has a spatial gradient due to boundaries. In the Poiseuille flow, phonons exhibit a maximum drift velocity at the center of a sample and a minimum drift velocity at the boundaries due to diffuse boundary scattering. With the spatial gradient of drift velocity from the center to the boundaries, the momentum of phonons is transferred through many N-scattering processes and finally destroyed by the diffuse boundary scattering, leading to thermal resistance.

*sylee@pitt.edu

The phonon Poiseuille flow has been theoretically studied [12,13] and experimentally confirmed by observing a peculiar temperature dependence of thermal conductivity that increases faster than the ballistic case [14]. For example, thermal conductivity of solid He was observed to follow the T^8 trend while the thermal conductivity of the ballistic limit should follow T^3. For suspended graphene, it has not been discovered yet if graphene exhibits a temperature dependence of thermal conductivity that is significantly different from the ballistic case so that the Poiseuille flow can be clearly observed in experiment. Recent studies qualitatively showed thermal conductivity of graphene that increases faster than the ballistic limit [5,15,16]. However, they relied on a simplified Callaway's scattering model [17,18] and some of them [15,16] used an empirical relation for scattering rates that was developed for three-dimensional materials [19,20], hindering quantitative guidance of future experimental efforts from first principles.

Here, we quantitatively discuss the details of the phonon Poiseuille flow in suspended graphene by solving the Peierls-Boltzmann equation (PBE). The past theoretical studies of the phonon Poiseuille flow [12,21,22] used the analytic solutions of the PBE to the first order, which is not valid when a sample size is not much larger than the MFP of N-scattering. The Navier-Stokes equation, based on a similar first-order solution of the molecular Boltzmann transport equation, requires for its validity that the width of the channel is larger than the MFP of intermolecular scattering by at least two orders of magnitudes (i.e., a molecular Knudesn number smaller than 0.01) [23]. Also, the scattering term is often simplified with Callaway's scattering model [10,16,12,21,22], which is not accurate for a quantitative purpose particularly when neither N- nor U-scattering is exceedingly larger than the other [18,24]. In this paper, we implement the deviational Monte Carlo method to solve the PBE to the higher order [25,26]. The phonon scattering is simulated with a full three-phonon scattering matrix from first principles without Callaway's model. Our simulation shows the peculiar temperature (T) and width (W) dependences of thermal conductivity in the hydrodynamic regime. Then we explain those peculiar dependences of thermal conductivity by introducing a concept of phonon hydrodynamic viscosity. The phonon hydrodynamic viscosity is derived from the PBE with Callaway's scattering model. It is worth pointing out that a similar effect has been recently discussed elsewhere as a friction effect induced on the relaxon gas [27] which is the eigenstates of a symmetrized phonon scattering matrix [28]. Here we use the conventional phonon concepts and formally derive the phonon hydrodynamic viscosity.

II. METHOD AND APPROACH

A. Monte Carlo simulation of the PBE

The PBE is a governing equation of phonon flow based on the assumption of phonon gas particles. With a linearized scattering term and the assumption of steady state, the PBE can be written as

$$\mathbf{v}_{\mathbf{q}s} \cdot \nabla_{\mathbf{r}} n_{\mathbf{q}s} = \sum_{\mathbf{q}'s'} C_{\mathbf{q}s,\mathbf{q}'s'} n^{\mathrm{d}}_{\mathbf{q}'s'} \tag{1}$$

where $n_{\mathbf{q}s}$ is the phonon distribution at the phonon state with wave vector $\mathbf{q}$ and polarization s. The $\mathbf{v}_{\mathbf{q}s}$ and $\mathbf{r}$ are the group velocity of the phonon and a position vector in real space, respectively. The $C_{\mathbf{q}s,\mathbf{q}'s'}$ is a scattering matrix of phonons and $n^{\mathrm{d}}_{\mathbf{q}s}$ is the deviation of the distribution function from the Bose-Einstein distribution ($n^0_{\mathbf{q}s}$), defined as $n_{\mathbf{q}s} - n^0_{\mathbf{q}s}$. This equation describes the balance of phonon distribution that is subject to advection (left-hand side) and scattering (right-hand side). The PBE is an integrodifferential equation with an integral term in the wave-vector space from the scattering and a differential term in the real space from the advection, together making this equation very challenging to solve.

The integral and differential terms in the PBE were often simplified with several assumptions to make the equation easier to solve. First, instead of using the full scattering matrix, $\mathbf{C}$, the off-diagonal terms of $\mathbf{C}$ are set to zero, eliminating the coupling between phonons through the scattering. This assumption, called the single-mode relaxation-time approximation (SMRT), describes the independent relaxation process of each phonon state; the corresponding phonon state exhibits relaxation from an out-of-equilibrium distribution to the equilibrium distribution while all other phonon states are kept at equilibrium. The SMRT eliminates the integration in the scattering term and is known to provide a reasonably accurate description for the phonon transport where the momentum-destroying U-scattering is a dominant scattering mechanism. However, the SMRT fails when N-scattering is dominant. Since the phonons in graphene exhibit strong N-scattering, the full scattering matrix should be used instead of the SMRT in this paper.

The second common approximation is to replace $\nabla_{\mathbf{r}} n_{\mathbf{q}s}$ with $\nabla_{\mathbf{r}} n^0_{\mathbf{q}s}$ where $n^0_{\mathbf{q}s}$ is the Bose-Einstein distribution. Further assuming a constant temperature gradient in the real-space domain, Eq. (1) can be simplified as

$$\mathbf{v}_{\mathbf{q}s} \cdot \nabla_{\mathbf{r}} T \frac{\partial n^0_{\mathbf{q}s}}{\partial T} = \sum_{\mathbf{q}'s'} C_{\mathbf{q}s,\mathbf{q}'s'} n^{\mathrm{d}}_{\mathbf{q}'s'}. \tag{2}$$

This homogenous approximation eliminates the differentiation in the advection term. With this assumption and the use of full scattering matrix, Eq. (2) was recently solved using an iterative method [3,5,8,29,30] or a variational approach [31]. The homogenous approximation is valid when the sample size is infinitely large or the spatial variation of the distribution function due to the diffuse boundary scattering is small enough to be ignored. In order to include the reduction of thermal conductivity due to the classical size effect, the boundary scattering rate is often calculated with a simple relation [8,32]:

$$\tau_{\mathrm{B}}^{-1} = \frac{2v_y}{W} \tag{3}$$

where v_y is the group velocity of the phonon in the normal direction to the boundary. Then, the calculated boundary scattering rate is added to the diagonal terms of the scattering matrix. Although the homogenous boundary scattering model can qualitatively predict the decreasing thermal conductivity as a sample size decreases, its assumption is not valid when phonon distribution significantly varies in space. In the phonon Poiseuille flow, we expect that the change of the distribution function along the normal direction to the temperature gradient is significant. This is because U-scattering, which provides spatially uniform momentum sink and thus causes a uniform

distribution function, is weaker than diffuse boundary scattering. Therefore, the homogenous approximation cannot be used for the hydrodynamic regime.

We use the deviational Monte Carlo method to solve Eq. (1) [25,26]. While a typical Monte Carlo method for solving the PBE samples the distribution function [33–35], the deviational Monte Carlo method samples the deviation of the distribution function from the already known equilibrium distribution [25,26]. As the deviation of distribution is significantly small compared to the distribution itself, sampling the deviation has much reduced stochastic uncertainty compared to sampling the distribution function. In addition, we solve the energy-based PBE instead of the PBE. The energy-based PBE can be obtained by multiplying phonon energy, $\hbar\omega$, on both sides of the PBE:

$$\mathbf{v}_{\mathbf{q}s} \cdot \nabla_{\mathbf{r}} f_{\mathbf{q}s} = \sum_{\mathbf{q}'s'} B_{\mathbf{q}s,\mathbf{q}'s'} f^{\mathrm{d}}_{\mathbf{q}'s'} \tag{4}$$

where f is the energy distribution function, a product of phonon energy ($\hbar\omega$) and distribution function ($n_{\mathbf{q}s}$). The matrix $B_{\mathbf{q}s,\mathbf{q}'s'}$ describes energy exchange due to scattering events, defined as $C_{\mathbf{q}s,\mathbf{q}'s'}\omega_{\mathbf{q}s}/\omega_{\mathbf{q}'s'}$. An advantage of solving the energy-based PBE is that the Monte Carlo simulation can strictly conserve total energy. If each sampling particle carries the same amount of deviational energy, the energy conservation can be satisfied by simply conserving the total number of particles [25].

The detailed algorithm of the deviational Monte Carlo method using a full scattering matrix can be found elsewhere [26] and here we briefly explain the algorithm. The deviational Monte Carlo simulation starts with initializing sample particles with an initial guess of distribution in both real and reciprocal spaces. Each particle carries a positive or negative value of unit deviational energy. The sample particles with a positive energy contribute to the distribution larger than the equilibrium case, and those with a negative energy contribute to the distribution smaller than the equilibrium case. Then, each particle flies with its group velocity during a given time interval. The occurrence of three-phonon scattering is stochastically determined with the full scattering matrix. This advection-scattering step is repeated until the particle distribution is converged.

As we use the full scattering matrix, our scattering algorithm differs from that in the case where SMRT is used [25,33–35]. Assuming an exponential decay of the phonon distribution function to equilibrium distribution (e.g., SMRT), a scattering probability, $P_{\mathbf{q}s}$, is calculated based on a relaxation time, $\tau_{\mathbf{q}s}$:

$$P_{\mathbf{q}s} = 1 - \exp\left(-\frac{\Delta t}{\tau_{\mathbf{q}s}}\right) \tag{5}$$

where Δt is the time interval. Then, a random number R is generated and compared to $P_{\mathbf{q}s}$, and phonon scattering occurs if R is smaller than $P_{\mathbf{q}s}$. However, with the full scattering matrix, we describe the change of phonon energy distribution during the given time interval with a matrix $\mathbf{P}$:

$$\mathbf{P}(\Delta t) = e^{\mathbf{B}\Delta t} = \sum_{k=0}^{\infty} \frac{\Delta t^k}{k!}\mathbf{B}^k. \tag{6}$$

The matrix $\mathbf{P}$ is defined such that the phonon energy distribution in the future time step is related to the distribution in the current time step as

$$f_i^{\mathrm{d}}(t+\Delta t) = \sum_j P_{ij}(\Delta t) f_j^{\mathrm{d}}(t) \tag{7}$$

where phonon state $\mathbf{q}s$ and $\mathbf{q}'s'$ are denoted as i and j for the sake of simplicity. Equation (7) is not adequate to be simulated using a stochastic method because $\mathbf{P}$ is a matrix with elements that can be negative or larger than unity. Equation (7) can be rewritten as a power series:

$$f_i^{\mathrm{d}}(t+\Delta t) = \sum_j \mathrm{sgn}[P_{ij}(\Delta t)]\frac{|P_{ij}(\Delta t)|}{p_j}\left[1+\sum_{n=1}^{\infty}\left(\frac{p_j^-}{p_j}\right)^n 2^n\right] f_j^{\mathrm{d}}(t) \tag{8}$$

where sgn is a sign function. The p_j and p_j^- are defined as

$$p_j = \sum_i |P_{ij}(\Delta t)|, \tag{9}$$

$$p_j^- = \sum_{i|P_{ij}(\Delta t)<0} |P_{ij}(\Delta t)|. \tag{10}$$

Note that $|P_{ij}(\Delta t)|/p_j$ and p_j^-/p_j range from zero to one and the sign of P_{ij} is shown in a separate sign function.

The power series in Eq. (8) can be stochastically simulated by implementing the following algorithm:

For a sampling particle in phonon state j

(1) Generate a random number R.

(2) Find the phonon state i satisfying

$$\sum_{k=1}^{i-1}\frac{|P_{kj}|}{P_j} \leqslant R < \sum_{k=1}^{i}\frac{|P_{kj}|}{P_j}. \tag{11}$$

The phonon state i can be found with a probability of $|P_{ij}(\Delta t)|/p_j$. Then, change the phonon state from j to i, and change the sign of energy the particle carries according to $\mathrm{sgn}[P_{ij}(\Delta t)]$.

(3) If $\mathrm{sgn}[P_{ij}(\Delta t)]$ is negative in step 2, this occurs with a probability of p_j^-/p_j and we simulate the term with the first order in p_j^-/p_j in Eq. (8). In this case, we simply generate two sampling particles in state j. Steps 1–3 are applied for these two particles. The terms with second and higher order in p_j^-/p_j in Eq. (8) can be recursively simulated during this process.

In this Monte Carlo simulation, we discretize time, real-space, and reciprocal space domains. The real-space domain is discretized into 20 control volumes along the width direction and one control volume along the length direction in which a small temperature gradient is applied. For the boundary parallel to the temperature gradient, fully diffuse boundary scattering is applied with an adiabatic boundary condition. For the boundary normal to the temperature gradient, a periodic boundary condition of heat flux [25,35] is applied because we assume the graphene sample is long enough such that the drift velocity does not change along the length direction, a so-called fully developed flow. The time interval between each advection-scattering step is determined from the three-phonon scattering rate such that the time interval is smaller than the minimum lifetime of the phonons with frequencies below $k_{\mathrm{B}}T/\hbar$ which contribute most of the heat flux. The reciprocal

space is sampled using a 40×40 grid. We confirmed that the calculation results converge well with respect to those discretization variables.

B. Momentum balance equation of phonons and phonon hydrodynamic viscosity

The momentum transfer through N-scattering to the boundaries combined with the diffuse boundary scattering, i.e., viscous damping effect, is the major source of thermal resistance in the hydrodynamic regime. Therefore, it would be interesting to define the phonon hydrodynamic viscosity which represents the rate of momentum transfer at a given drift velocity gradient. Here we derive the expression for the phonon hydrodynamic viscosity and the momentum balance equation from the PBE with Callaway's scattering model. We assume that the MFP of N-scattering is much smaller than the characteristic sample size. The steady-state PBE with Callaway's scattering model is

$$\mathbf{v}_{\mathbf{q}s}\cdot\nabla_{\mathbf{x}}n_{\mathbf{q}s}=-\frac{n_{\mathbf{q}s}-n_{\mathbf{q}s}^{\mathrm{disp}}}{\tau_{\mathrm{N}\mathbf{q}s}}-\frac{n_{\mathbf{q}s}-n_{\mathbf{q}s}^{0}}{\tau_{\mathrm{U}\mathbf{q}s}}. \tag{12}$$

Here $n_{\mathbf{q}s}^{\mathrm{disp}}$ is the displaced Bose-Einstein distribution defined as

$$n_{\mathbf{q}s}^{\mathrm{disp}}=\frac{1}{\exp\left[\frac{\hbar(\omega_{\mathbf{q}s}-q_\alpha u_\alpha)}{k_{\mathrm{B}}(T_0+\Delta T)}\right]-1} \tag{13}$$

where q_α and u_α are the wave vector and the drift velocity along the direction of α, respectively. The ΔT represents the deviation of local equilibrium temperature from global equilibrium temperature T_0. Equation (13) can be linearized as

$$n_{\mathbf{q}s}^{\mathrm{disp}}=n_{\mathbf{q}s}^{0}+n_{\mathbf{q}s}^{0}\left(n_{\mathbf{q}s}^{0}+1\right)\frac{\hbar\omega_{\mathbf{q}s}}{k_{\mathrm{B}}T_0}T'+n_{\mathbf{q}s}^{0}\left(n_{\mathbf{q}s}^{0}+1\right)\frac{\hbar q_\alpha u_\alpha}{k_{\mathrm{B}}T_0} \tag{14}$$

by assuming $q_\alpha u_\alpha \ll \omega$, and $T'=\Delta T/T_0 \ll 1$ where T' is the ratio of temperature difference to the equilibrium temperature. The momentum balance equation can be derived by multiplying q_x on both sides of Eq. (12) and integrating over the first Brillouin zone. The resulting equation is

$$\frac{d\Theta_{xx}}{dx}+\frac{d\Theta_{xy}}{dy}=\frac{1}{(2\pi)^2}\sum_s\int q_x\left(-\frac{n_{\mathbf{q}s}-n_{\mathbf{q}s}^{0}}{\tau_{\mathrm{U}\mathbf{q}s}}\right)d\mathbf{q} \tag{15}$$

where

$$\Theta_{xx}=\frac{1}{(2\pi)^2}\sum_s\int q_x v_{x\mathbf{q}s}n_{\mathbf{q}s}d\mathbf{q}, \tag{16}$$

$$\Theta_{xy}=\frac{1}{(2\pi)^2}\sum_s\int q_x v_{y_{\mathbf{q}s}}n_{\mathbf{q}s}d\mathbf{q}. \tag{17}$$

The Θ_{xx} and Θ_{xy} represent the flux along x and y directions, respectively, of x-direction momentum in a two-dimensional material. Note that the momentum change due to scattering in the right-hand side includes only U-scattering because N-scattering conserves total momentum.

The distribution function in Θ_{xx} and Θ_{xy} can be found by solving Eq. (12) with the following approximation:

$$\nabla_{\mathbf{x}}n_{\mathbf{q}s}\approx\nabla_{\mathbf{x}}n_{\mathbf{q}s}^{\mathrm{disp}}, \tag{18}$$

which corresponds to the first order in Chapman-Enskog expansion of gas kinetics theory [23] and is also called the mean free time approximation. This approximation is valid if the phonon MFP is much smaller than the characteristic length of a sample. Applying the mean free time approximation to Eq. (12) gives

$$\mathbf{v}_{\mathbf{q}s}\cdot\nabla_{\mathbf{x}}n_{\mathbf{q}s}^{\mathrm{disp}}=-\frac{n_{\mathbf{q}s}-n_{\mathbf{q}s}^{\mathrm{disp}}}{\tau_{\mathrm{N}\mathbf{q}s}}-\frac{n_{\mathbf{q}s}-n_{\mathbf{q}s}^{0}}{\tau_{\mathrm{U}\mathbf{q}s}}. \tag{19}$$

Inserting the solution of Eqs. (19) into (15) and assuming the fully developed flow case $du_x/dx=0$ gives

$$\frac{dT'}{dx}=\mu_{\mathrm{ph}}\frac{\partial^2 u_x}{\partial y^2}-\beta u_x \tag{20}$$

where

$$\mu_{\mathrm{ph}}=\frac{\left[\sum_s\int q_x^2 v_{y_{\mathbf{q}s}}^2 n_{\mathbf{q}s}^{0}\left(n_{\mathbf{q}s}^{0}+1\right)\tau_{\mathrm{N}\mathbf{q}s}d\mathbf{q}\right]}{\left[\sum_s\int q_x v_{x\mathbf{q}s}n_{\mathbf{q}s}^{0}\left(n_{\mathbf{q}s}^{0}+1\right)\omega_{\mathbf{q}s}d\mathbf{q}\right]}, \tag{21}$$

$$\beta=\frac{\left[\sum_s\int q_x^2 n_{\mathbf{q}s}^{0}\left(n_{\mathbf{q}s}^{0}+1\right)\tau_{\mathrm{U}\mathbf{q}s}^{-1}d\mathbf{q}\right]}{\left[\sum_s\int q_x v_{x\mathbf{q}s}n_{\mathbf{q}s}^{0}\left(n_{\mathbf{q}s}^{0}+1\right)\omega_{\mathbf{q}s}d\mathbf{q}\right]}. \tag{22}$$

Here we assume $\tau_{\mathrm{N}\mathbf{q}s}^{-1}\gg\tau_{\mathrm{U}\mathbf{q}s}^{-1}$. Equation (20) can be understood as a momentum balance of the phonon system: the phonon system gains net momentum from the temperature gradient in the left-hand side and the gained momentum is either spatially distributed by the viscous effect represented by phonon viscosity (μ_{ph}) or destroyed by U-scattering represented by β. A similar equation was provided elsewhere [5] without derivation. Note that the momentum balance equation in the previous work [5] includes $|\mathbf{v}|^2$ in the viscosity, but it should be corrected to v_y^2. The thermal conductivity can then be calculated by solving Eq. (20) with an assumption of zero drift velocity at the boundary (so-called no-slip boundary condition) and the assumption of negligible U-scattering [5]:

$$\kappa_{\mathrm{drift}}=\frac{\hbar^2}{48k_{\mathrm{B}}\pi^2}\frac{\sum_s\int\omega_{\mathbf{q}s}q_x v_{x\mathbf{q}s}n_{\mathbf{q}s}^{0}\left(n_{\mathbf{q}s}^{0}+1\right)d\mathbf{q}}{\mu_{\mathrm{ph}}T_0^2}W^2. \tag{23}$$

III. RESULTS AND DISCUSSION

A. Temperature dependence of thermal conductivity

The temperature dependence of thermal conductivity is different for all three regimes of phonon transport. The thermal conductivity in the diffusive regime decreases with temperature due to the increased rates of U-scattering. In the ballistic regime, thermal conductivity follows the trend of the ballistic thermal conductance, $C_{\mathrm{V}}v$, where C_{V} is the volumetric specific heat and v is the phonon group velocity. The ballistic thermal conductance of three-dimensional debye crystal increases as T^3, since the phonon group velocity is a constant and the specific heat increases with T^3 at temperatures below the debye temperature. However, in the hydrodynamic regime, thermal conductivity was found to increase with temperature faster than the ballistic case [12–14]. This unique temperature dependence in the hydrodynamic regime was used to experimentally confirm the steady-state hydrodynamic flow of phonons. In a past study, the thermal conductivity of solid He increases as

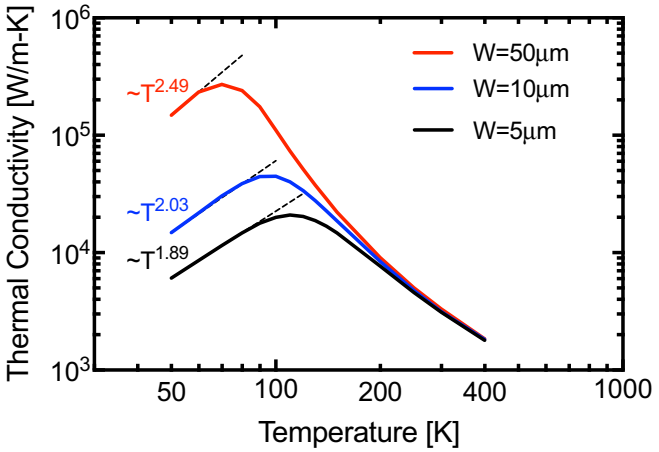

FIG. 1. Temperature dependence of thermal conductivity for different sample widths. The dashed lines represent the exponential fit of the results. Thermal conductivity increases faster than the ballistic case as temperature increases, indicating phonon Poiseuille flow. The exponent of temperature is obtained by fitting the data from 50 to 80 K (5 and 10 μm) and from 50 to 60 K (50 μm).

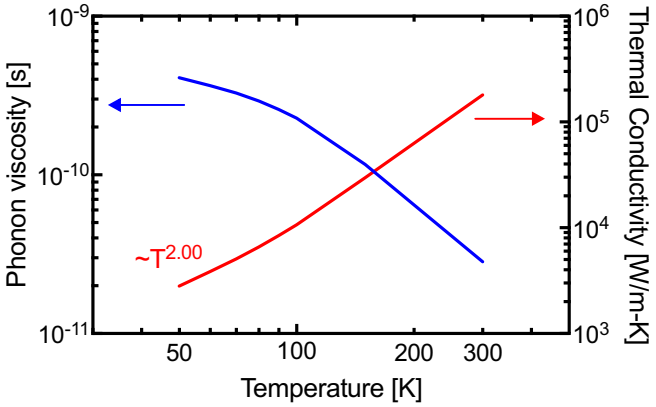

FIG. 2. Temperature dependence of phonon viscosity and thermal conductivity. The phonon viscosity decreases with temperature, resulting in thermal conductivity increasing with temperature faster than the ballistic case. The exponent of temperature is obtained by fitting the data in the temperature range from 50 to 100 K.

T^8 at low temperature, much different from the T^3 trend of the ballistic case [14]. For the experimental confirmation of the phonon Poiseuille flow in graphene, it would be important to see if the thermal conductivity of graphene exhibits a peculiar temperature dependence that is clearly distinguished from the ballistic case.

In Fig. 1, we show the temperature dependence of thermal conductivity in suspended graphene from the Monte Carlo simulation. Note that the ballistic thermal conductance in graphene increases as $T^{1.68}$, different from the three-dimensional debye crystal case [4]. This is because graphene has a flexural acoustic phonon branch that has a quadratic dispersion relation in a two-dimensional space. In Fig. 1, it is observed that thermal conductivity increases with temperature faster than that of the ballistic transport in the temperature range from 50 to 100 K. The temperature dependence of thermal conductivity in this temperature range varies from $T^{1.89}$ to $T^{2.49}$ for different widths, which is clearly distinguished from the trend of $T^{1.68}$ of the ballistic case. When a temperature is larger than 100 K, the thermal conductivity decreases with temperature due to the increased U-scattering rate.

The fact that thermal conductivity increases with temperature faster than the ballistic case can be understood using the kinetic theory combined with a simple random-walk theory [12,13]. According to the kinetic theory, thermal conductivity is proportional to $C_V v L_{\text{eff}}$, where L_{eff} is the effective MFP of phonons, i.e., the total travel distance until a phonon particle encounters a momentum-destroying scattering process. In purely ballistic transport with fully diffuse boundary scattering, there is no internal phonon scattering and L_{eff} is fixed at the characteristic size of a sample. Therefore, the thermal conductivity in this case follows the same trend of the ballistic thermal conductance that increases as $T^{1.68}$. When the transport is in the ideal hydrodynamic regime, i.e., N-scattering is significantly strong and U-scattering is negligibly weak compared to the diffuse boundary scattering, the boundary cannot be seen directly by phonon particles, but screened by many N-scattering processes. This circumstance can be roughly described by a random walk of phonon particles experiencing N-scattering processes. Then, L_{eff} is W^2/Λ_N, where Λ_N is the MFP for N-scattering. As temperature increases, Λ_N decreases due to the increased N-scattering, making L_{eff} larger, while L_{eff} is a constant in the ballistic transport. Therefore, the thermal conductivity in the hydrodynamic regime changes with T^α where α is larger than 1.68 of the ballistic case.

This temperature dependence can also be explained by the momentum balance equation [Eq. (20)] and the concept of phonon hydrodynamic viscosity. The phonon hydrodynamic viscosity is inversely proportional to the N-scattering rate according to Eq. (21), meaning that a momentum transfer rate decreases as N-scattering becomes stronger. This observation agrees with the aforementioned random-walk picture. With higher N-scattering rate, the boundary can be more effectively screened and the momentum transfer rate to the boundary becomes less. Therefore, if the viscous damping effect is the major contributor to thermal resistance, strong N-scattering can decrease thermal resistance. In Fig. 2, we present the phonon hydrodynamic viscosity of suspended graphene that is calculated with phonon dispersion and scattering rates from the first-principles calculation. The phonon hydrodynamic viscosity decreases with temperature because N-scattering rate is increased. Thus, the thermal conductivity should exhibit a steep increase with temperature if the viscous damping effect significantly contributes to the total thermal resistance. We show the temperature dependence of thermal conductivity [Eq. (23)] in Fig. 2. The calculated thermal conductivity from the momentum balance equation increases approximately as T^2, similar to our Monte Carlo results shown in Fig. 1.

It should be noted from Eq. (23) that thermal conductivity is inversely proportional to hydrodynamic viscosity. As viscosity decreases, viscous damping becomes smaller and thermal conductivity can be larger, as shown in Fig. 2. Equation (23) also indicates that thermal conductivity should have the same exponent value of temperature regardless of widths. This

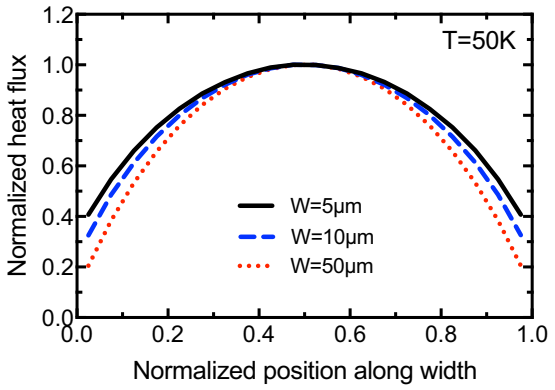

FIG. 3. Normalized heat flux profile at 50 K, for sample widths of 5, 10, and 50 μm. The displacements near the boundaries are not zero and increase as a width decreases. The nonzero displacements indicate slip boundary condition.

contradicts to our results from the Monte Carlo solution shown in Fig. 1. It is observed in Fig. 1 that different widths result in different values of exponent; the exponent value increases with a width. The exponent value from our Monte Carlo simulation depends on a width because the no-slip boundary condition assumed in Eq. (23) is not completely satisfied in the actual cases. The normalized heat flux profile in Fig. 3 shows nonzero heat flux near the boundaries. The heat flux near the boundaries becomes larger as a width becomes smaller.

This slip boundary condition occurs due to a ballistic effect. In the limit of very strong N-scattering and very short MFP of N-scattering, the displacement near the boundary should approach zero. However, if MFP of N-scattering is not much smaller than the width, the displacement can be larger than zero, due to the contributions of phonons travelled without scattering from the center of a sample where the displacement is large. The slip displacement reduces the viscous damping effect by flattening the heat flux profile. This can lead to a smaller exponent value of temperature in the thermal conductivity shown in Fig. 1.

The role of viscous damping effect in thermal resistance can also be found from the shape of the heat flux profile. The heat flux profile shape is almost uniform when U-scattering is the major source for the thermal resistance as U-scattering can occur at any place of a sample. However, when the viscous damping by N-scattering is important, the heat flux profile varies in space and the momentum transfer along the drift velocity gradient can occur. In Fig. 4(a), we present the profiles of local thermal conductivity, i.e., heat flux per temperature gradient, at 100 and 300 K. At 300 K, the local thermal conductivity is almost constant in the entire cross-section, indicating that the direct destruction of momentum by U-scattering is the largest contributor to the total thermal resistance. At 100 K, the local thermal conductivity nearly follows the parabolic shape that is observed in molecular Poiseuille flow. Due to the drift velocity gradient, momentum can be transferred to the wall through many N-scattering events. In this case, the thermal resistance is mostly due to the viscous damping effect, as also can be seen from the peculiar temperature dependence of thermal conductivity shown in Fig. 1.

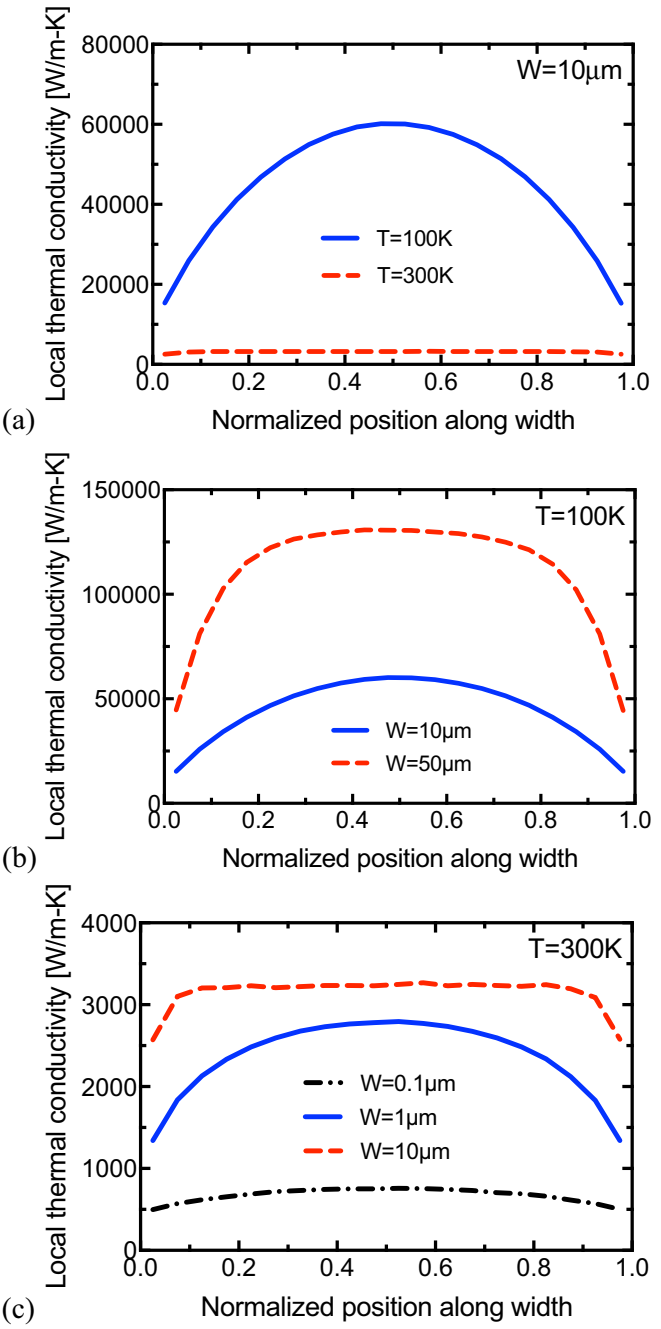

FIG. 4. Local thermal conductivity profile from the Monte Carlo simulation under different conditions: (a) 100 and 300 K for a 10 μm-wide sample, (b) sample widths of 10 and 50 μm at 100 K, and (c) sample widths of 0.1, 1, and 10 μm at 300 K.

B. Sample width dependence of thermal conductivity

All three transport regimes exhibit different behavior of thermal conductivity changes as a sample width changes. In the ballistic regime, phonon MFP is limited to the characteristic sample size, thus thermal conductivity increases linearly with a width. In the diffusive regime, thermal conductivity does not change with a width. In contrast, thermal conductivity in the hydrodynamic regime increases superlinearly with a sample width [4,5,15,16]. In the ideal hydrodynamic regime where there is no U-scattering and a sample size is much larger

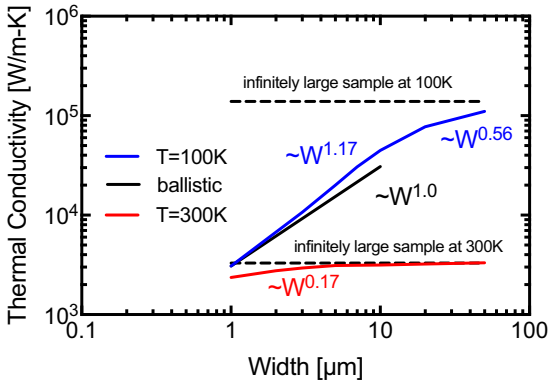

FIG. 5. Sample width dependence of thermal conductivity at 100 and 300 K. The dashed lines represent the thermal conductivities for an infinitely large sample. The black solid line represents the ballistic case, where thermal conductivity is linearly proportional to a width. The thermal conductivity at 100 K superlinearly increases with a width, indicating the significant hydrodynamic regime.

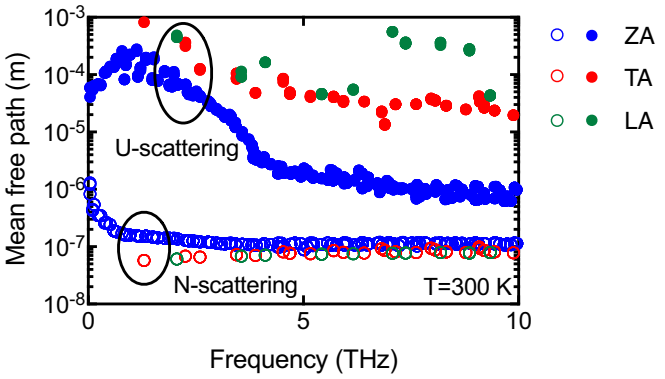

FIG. 6. Comparison of MFPs of N- and U-scatterings at 300 K. The filled circles are for U-scattering and the void circles are for N-scattering.

than the MFP of N-scattering, thermal conductivity should increase as W^2 [5]. This can be easily shown from the random-walk picture or the momentum balance equation [Eq. (20)], assuming there is no U-scattering. However, with the existence of U-scattering, thermal conductivity would follow the trend of W^α where α is less than 2.

In Fig. 5, we present the dependence of thermal conductivity on sample widths from our Monte Carlo simulation. At 300 K, thermal conductivity depends on sample widths very weakly; the width dependence is $W^{0.17}$ in the range of width from 1 to 5 μm. For widths larger than 5 μm, the thermal conductivity is almost the same as the thermal conductivity of an infinitely large sample. This suggests that the momentum destruction by U-scattering is stronger than the viscous damping effect at 300 K.

In contrast, the thermal conductivity at 100 K clearly shows a superlinear increase with a width; the dependence is $W^{1.17}$ in the range of widths from 1 to 10 μm. As a width is further increased, the width dependence is weaker, showing a sublinear dependence. The transition from the strong dependence $W^{1.17}$ to the weak dependence $W^{0.56}$ at 100 K can be explained by the relative strength of viscous damping and U-scattering. At a fixed temperature, the thermal resistance by U-scattering is constant regardless of widths. However, the viscous damping effect varies with sample widths. From the momentum balance equation, the momentum transfer rate is proportional to hydrodynamic phonon viscosity and the gradient of drift velocity. As a width increases, the gradient of drift velocity is decreased, making the viscous damping effect smaller. When a width is between 1 and 10 μm, the viscous damping effect is relatively stronger than the momentum destruction by U-scattering, giving the superlinear dependence of thermal conductivity on widths. However, as a width further increases, the viscous damping effect decreases, and the transport regime becomes closer to the diffusive limit. This behavior can be also seen in the local thermal conductivity profile shown in Fig. 4(b). When a width is 10 μm, the local thermal conductivity has nearly parabolic profile shape, indicating that the viscous damping is the major source of thermal resistance. However, when a width is 50 μm, the local thermal conductivity profile is flattened and the momentum transfer to the wall is relatively insignificant compared to the 10-μm case.

C. Transition from hydrodynamic to diffusive regimes

We have focused on the peculiar behaviors of thermal conductivity at 100 K where the hydrodynamic regime is dominant over other regimes. Although the 300 K case does not exhibit the peculiar behaviors of temperature- and width-dependent thermal conductivity of the hydrodynamic regime, the MFP of N-scattering is still significantly smaller than those of U-scattering as shown in Fig. 6. This suggests that N-scattering and the resulting viscous damping may still play an important role in the thermal transport.

In Fig. 7, we compare the thermal conductivity values from two different methods. One is from our Monte Carlo solution where we consider the spatial variation of phonon distribution and solve the PBE in both real and reciprocal spaces (hereafter κ_{MC} represents the thermal conductivity values from the Monte

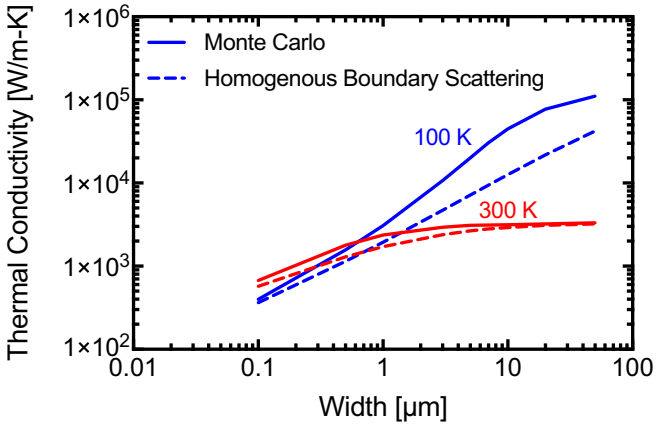

FIG. 7. Comparison of thermal conductivity values with different boundary scattering models: spatially nonhomogenous boundary scattering by Monte Carlo simulation of the PBE (solid line) and spatially homogenous boundary scattering (dashed line). The difference between them shows the significance of the viscous damping effect.

Carlo solution). The other is from the iterative solution where we ignore the spatial variation of phonon distribution and assume a simple homogenous boundary scattering [8] (hereafter κ_{homo} represents the thermal conductivity values from the homogenous boundary scattering). This comparison was reported in two recent papers [16,27] and the difference between the two methods was used to explain the friction effects in the relaxon framework [28]. Here we use the conventional phonon concept to explain the difference. In the homogenous boundary scattering model [Eq. (3)], the boundary scattering acts like a momentum sink that is homogenously distributed in space, and its rate is based on the assumption of ballistic transport to the boundary. Therefore, the homogenous boundary scattering model cannot capture the viscous damping effect that occurs due to many N-scattering events and the gradient of drift velocity. As the homogenous boundary scattering assumes that the phonon particles directly see the boundary, it overestimates thermal resistance compared to the actual case where the boundary is screened by many N-scattering events.

It is found in Fig. 7 that κ_{MC} is significantly larger than κ_{homo} at 100 K where we predicted the hydrodynamic regime is dominant over other regimes. In this case, the viscous damping is the major contributor to the thermal resistance, and therefore the homogenous boundary scattering model cannot accurately predict the thermal conductivity values. When a width is very small (0.1 μm) or exceedingly large (>50 μm) representing the cases that are close to the ballistic or diffusive limits, respectively, the difference between κ_{MC} and κ_{homo} is small. It is noteworthy that κ_{MC} is larger than κ_{homo} by 40% even at 300 K where the peculiar temperature and width dependences of thermal conductivity in the hydrodynamic regime do not exist. This indicates that the viscous damping effect can still play an important role at 300 K, even though the transport is not clearly in the hydrodynamic regime but in between the hydrodynamic and diffusive limits.

The phonon distribution and heat flux profile also support that the viscous damping effect is still important at 300 K. For the hydrodynamic viscosity to be well defined, a collective motion of phonon particles with the same drift velocity is necessary. We show in Fig. 8 that the phonon particles at 300 K form a clear collective motion. The slope in Fig. 8 represents the drift velocity of each phonon state. It is clear that all phonon modes in the phonon states with small wave vectors which contribute most of the heat flux, exhibit the same drift velocity regardless of phonon wave vector and polarization. In addition, the local thermal conductivity profile in Fig. 4(c) also indicates that viscous damping effect can be significant at 300 K when a width is around 1 μm. The local thermal conductivity profile in this case exhibits a large gradient along the width direction, indicating that the viscous damping effect can be significant. However, when a width is 0.1 or 10 μm, the local thermal conductivity profile is almost uniform and the viscous damping effect is almost negligible.

IV. SUMMARY AND CONCLUSIONS

We have discussed the hydrodynamic phonon transport in suspended graphene using the Monte Carlo solution of the PBE in both real and reciprocal spaces. Our solution of the PBE is based on the deviational Monte Carlo method using the full scattering matrices from first-principles lattice dynamics calculation, and thus holds the predictive power of the first-principles calculations. We focus on the peculiar temperature and width dependences of thermal conductivity when the hydrodynamic regime is dominant over the diffusive and ballistic regimes. The calculation shows that thermal conductivity values follow the trends of T^{α} where α ranges from 1.89 to 2.49, and $W^{1.17}$ when a temperature is around 100 K and widths are from 1 to 10 μm. These behaviors are clearly distinguishable from those of the ballistic and diffusive limits, and thus can serve as an indicator of the hydrodynamic regime. Our calculation results can be used to guide future experimental studies to confirm the phonon Poiseuille flow.

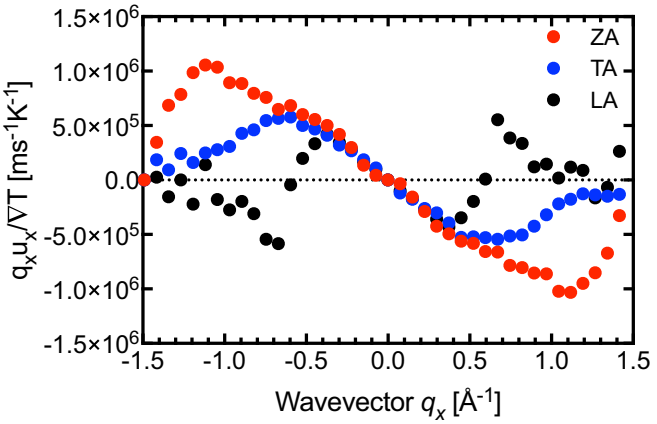

FIG. 8. Deviation of phonon distribution from the equilibrium case from Monte Carlo simulation of the PBE. The phonon distribution is sampled at the center of a 1-μm-wide sample at 300 K. The slope between two adjacent phonon states (circles) represents the drift velocity at the phonon state.

The peculiar behaviors of thermal conductivity are qualitatively explained with the concept of phonon hydrodynamic viscosity. We derived a momentum balance equation from the PBE using Callaway's scattering model to separate N- and U-scatterings, and defined the phonon hydrodynamic viscosity. It is found that the hydrodynamic viscous damping is a significant contributor to thermal resistance at 100 K where the hydrodynamic regime is dominant. The viscous damping effect still plays an important role in thermal transport when a temperature is 300 K and a width is around 1 μm, even though the transport regime in this condition is not clearly hydrodynamic but in a transition between the hydrodynamic and diffusive regimes.

ACKNOWLEDGMENTS

We acknowledge support from NSF Grants No. 1705756 and No. 1709307. This paper was also supported by the Central Research Development Fund of University of Pittsburgh (Grant No. 9012883). This paper used the clusters of Extreme Science and Engineering Discovery Environment through Allocation No. TG-PHY170010 and clusters of Center for Research Computing at University of Pittsburgh.

[1] A. A. Balandin, S. Ghosh, W. Bao, I. Calizo, D. Teweldebrhan, F. Miao, and C. N. Lau, Nano Lett. **8**, 902 (2008).
[2] J. H. Seol, I. Jo, A. L. Moore, L. Lindsay, Z. H. Aitken, M. T. Pettes, X. Li, Z. Yao, R. Huang, D. Broido, N. Mingo, R. S. Ruoff, and L. Shi, Science **328**, 213 (2010).
[3] L. Lindsay, D. A. Broido, and N. Mingo, Phys. Rev. B **80**, 125407 (2009).
[4] M.-H. Bae, Z. Li, Z. Aksamija, P. N. Martin, F. Xiong, Z.-Y. Ong, I. Knezevic, and E. Pop, Nat. Commun. **4**, 1734 (2013).
[5] S. Lee, D. Broido, K. Esfarjani, and G. Chen, Nat. Commun. **6**, 6290 (2015).
[6] A. Cepellotti, G. Fugallo, L. Paulatto, M. Lazzeri, F. Mauri, and N. Marzari, Nat. Commun. **6**, 6400 (2015).
[7] P. K. Schelling and P. Keblinski, Phys. Rev. B **68**, 035425 (2003).
[8] L. Lindsay, D. A. Broido, and N. Mingo, Phys. Rev. B **82**, 115427 (2010).
[9] S. Lee and L. Lindsay, Phys. Rev. B **95**, 184304 (2017).
[10] Z. Ding, J. Zhou, B. Song, V. Chiloyan, M. Li, T.-H. Liu, and G. Chen, Nano Lett. **18**, 638 (2018).
[11] J. M. Ziman, *Electrons and Phonons: The Theory of Transport Phenomena in Solids* (Oxford University Press, London, 1960).
[12] R. A. Guyer and J. A. Krumhansl, Phys. Rev. **148**, 778 (1966).
[13] R. N. Gurzhi, J. Exp. Theor. Phys. **46**, 719 (1964).
[14] L. P. Mezhov-Deglin, J. Exp. Theor. Phys. **49**, 66 (1965).
[15] A. K. Majee and Z. Aksamija, Phys. Rev. B **93**, 235423 (2016).
[16] Y. Guo and M. Wang, Phys. Rev. B **96**, 134312 (2017).
[17] J. Callaway, Phys. Rev. **113**, 1046 (1959).
[18] P. B. Allen, Phys. Rev. B **88**, 144302 (2013).
[19] D. T. Morelli, J. P. Heremans, and G. A. Slack, Phys. Rev. B **66**, 195304 (2002).
[20] G. A. Slack and S. Galginaitis, Phys. Rev. **133**, A253 (1964).
[21] R. A. Guyer and J. A. Krumhansl, Phys. Rev. **148**, 766 (1966).
[22] J. A. Sussmann and A. Thellung, Proc. Phys. Soc. **81**, 1122 (1963).
[23] W. G. Vincenti and C. H. Kruger, *Introduction to Physical Gas Dynamics* (Wiley, New York, 1965).
[24] J. Ma, W. Li, and X. Luo, Phys. Rev. B **90**, 035203 (2014).
[25] J. P. M. Péraud and N. G. Hadjiconstantinou, Phys. Rev. B **84**, 205331 (2011).
[26] C. D. Landon and N. G. Hadjiconstantinou, J. Appl. Phys. **116**, 163502 (2014).
[27] A. Cepellotti and N. Marzari, Nano Lett. **17**, 4675 (2017).
[28] A. Cepellotti and N. Marzari, Phys. Rev. X **6**, 041013 (2016).
[29] A. Ward, D. A. Broido, D. A. Stewart, and G. Deinzer, Phys. Rev. B **80**, 125203 (2009).
[30] M. Omini and A. Sparavigna, Phys. Rev. B **53**, 9064 (1996).
[31] G. Fugallo, M. Lazzeri, L. Paulatto, and F. Mauri, Phys. Rev. B **88**, 045430 (2013).
[32] P. Carruthers, Rev. Mod. Phys. **33**, 92 (1961).
[33] R. B. Peterson, J. Heat Transfer **116**, 815 (1994).
[34] S. Mazumder and A. Majumdar, J. Heat Transfer **123**, 749 (2001).
[35] Q. Hao, G. Chen, and M. S. Jeng, J. Appl. Phys. **106**, 114321 (2009).